IEEE Access
Multidisciplinary | Rapid Review | Open Access Journal

Received December 19, 2019, accepted February 18, 2020, date of publication February 24, 2020, date of current version March 3, 2020.

Digital Object Identifier 10.1109/ACCESS.2020.2976104

Harmonic Multiple Loop Detection (HMLD) Algorithm for Not-Contact Vital Sign Monitoring Based on Ultra-Wideband (UWB) Radar

YI ZHANG, XIUPING LI, (Senior Member, IEEE), RUI QI, ZIHANG QI, (Student Member, IEEE), AND HUA ZHU, (Member, IEEE)

School of Electronic Engineering, Beijing University of Posts and Telecommunications, Beijing 100876, China
Key Laboratory of Universal Wireless Communications, Ministry of Education, Beijing 100876, China
Beijing Key Laboratory of Work Safety Intelligent Monitoring, Beijing 100876, China

Corresponding author: Xiuping Li (xpli@bupt.edu.cn)

ABSTRACT In this paper, the harmonic multiple loop detection (HMLD) algorithm for heart rate (HR) and respiration rate (RR) estimation with impulse radio ultrawideband (IR-UWB) radar is introduced. The algorithm includes two parts: one is the harmonic multiple discriminant principle and the other is the cyclic spectrum updating process. The harmonic multiple discriminant principle is used to detect whether the peak point in the fundamental frequency band is the true vital sign signal. The cyclic spectrum updating process can remove the error peak point according to the results obtained from the part one. In this algorithm, threshold setting is not needed and the estimation error caused by the erroneous threshold can be reduced. Only the fundamental and second harmonic frequencies are needed for HR and RR estimation, so the algorithm has strong environmental robustness and low requirement of radar hardwares. Compared with other algorithms, HMLD algorithm provides reasonable average error rates (4.95% and 5.06%) compared to real data from the oximeter in RR and HR detection. The real-time vital signs detection experiment shows that HMLD algorithm can not only detect the vital signs rate and record the historical curve in real time, but also detect the location information, which proves the validity of HMLD algorithm in real-time vital signs detection.

INDEX TERMS Harmonic multiple loop detection, biomedical signal processing, impulse radio ultrawideband (IR-UWB) radar, heart rate (HR), respiration rate (RR).

I. INTRODUCTION

Vital sign detection is an essential part of the medical, health care and military field. By measuring respiratory rate (RR) and heart rate (HR), medical staff can diagnose clinical disease for patients and monitor disease through vital signs [1]–[5]. In the health monitor of infants and the elderly, monitoring vital signs can observe physical changes and sleep quality, which plays a role in preventing sudden disease [6], [7]. The current common method of detecting vital signs is to contact the human body to obtain vital signs information, such as pulse-oximetry and electrocardiogram (ECG). However, for those who are not suitable for skin contact, such as burn patients or newborns, contact vital sign detection equipment cannot be applied. In the case of long-term monitoring, contact vital sign detection equipment is inconvenient and uncomfortable. Therefore, it is necessary to study the non-contact vital sign detection method.

There are many types of equipment for target detection and extraction of vital signs. One of them is the imaging device system. The image processing algorithm estimates HR and RR by measuring the color change of reflected light [8]–[14]. Although this equipment can achieve the estimation of HR and RR, it requires adequate illumination and an uncovered measurement environment, which imposes limitations on non-contact vital sign detection applications. The non-contact vital sign detection method based on radar system makes up for the above limitations [15]. Radar systems for non-contact vital sign detection have multiple options [16]–[26]. Compared with other types of radars, IR-UWB

The associate editor coordinating the review of this manuscript and approving it for publication was Dian Tjondronegoro.

radar has the characteristics of low-power, anti-interference, multipath resistance and high penetration [22]–[24]. The pulse characteristics of the UWB radar not only enable low-power performance, but also allow high-resolution positioning and sensing, which has great advantages in applications such as target detection of hidden objects, recognition of respiratory and heartbeat signals, and close-range data transmission. When detecting vital signs, the UWB radar transmits a series of short-time low-power pulses to the subject, which are reflected back by the body later. Since the respiration and heartbeat cause periodic motion of the chest wall, the radar echo signal carries information about respiration and heartbeat [25], [26]. The correlation algorithm can extract the vital signs information of the subject by analyzing the radar echo signals.

Many algorithms for non-contact vital sign detection based on UWB radar have been proposed [3], [23], [27]–[35]. Traditional spectral analysis algorithms extract RR and HR by converting the filtered slow-time signals into a spectrum and then analyzing the peaks in the spectrum [27], [28]. Further more, some complex algorithms for respiratory heartbeat detection based on UWB radar were proposed. T. Sakamoto used an algorithm based on continuous wavelet filtering and ensemble empirical mode decomposition (EEMD) to extract the heart and lung signals [32]. Then ZhenZhen Duan used the variational mode decomposition (VMD) algorithm to extract heartbeat signals and respiratory signals [23]. In addition, PengFei Wang proposed to apply convolutional sparse coding to the application of breathing heartbeat algorithm [3]. The above algorithms realize the extraction of RR and HR. However, Due to complex algorithm steps, it is not suitable for real-time vital sign detection. In pursuit of simple calculations and high accuracy, many algorithms using harmonic components were proposed to detect the RR and HR. Nguyen proposed the harmonic path (HAPA) algorithm and the spectral-averaged harmonic path detection (SHAPA) algorithm for detecting the frequency of respiration and heartbeat [29], [30]. The HAPA algorithm detects the frequency of the breath and heartbeat by finding the harmonic path in spectrogram. However, since three or more harmonics are difficult to extract, there is a problem that the harmonic path cannot be recognized using the HAPA algorithm. The SHAPA algorithm adds spectrum averaging processing to solve the issue that the harmonic path cannot be identified. Then Elliott Schires used the SHAPA, power spectral density algorithm and state space method to detect the driver's breathing rate and heart rate in a car [31].

In this paper, in order to reduce the test environmental and equipment requirements while ensuring high accuracy and simple calculations, a new harmonic multiple loop detection (HMLD) algorithm for non-contact vital sign detection is proposed. The new algorithm only needs to extract the fundamental and the second harmonic component, and does not need to set the threshold. It not only utilizes the harmonic component of the respiratory and heartbeat signal, but also reduces the detection error caused by the inability to detect the path and the threshold setting.

The paper is organized as follows: Section II describes the specific content of radar signal processing and HMLD algorithm. Section III describes the experimental content of RR and HR estimation using HMLD algorithm and the real-time detection of vital signs. Experimental results and conclusion are presented in Section IV and V.

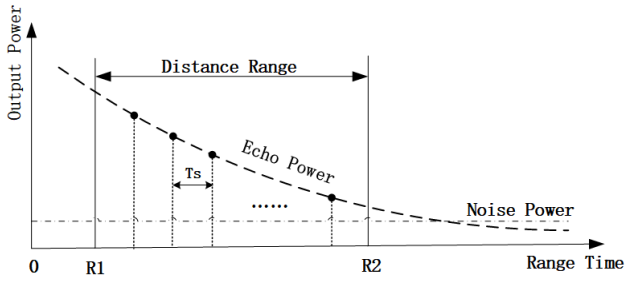

FIGURE 1. Power variation image of UWB radar pulse signal [36].

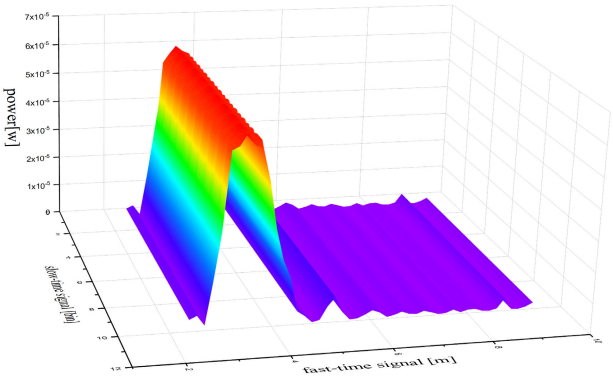

FIGURE 2. Three-dimensional image of UWB radar echo signal. The x and z axes represent fast-time signals, and the y and z axes represent slow-time signals [37].

II. HARMONIC MULTIPLE LOOP DETECTION (HMLD) ALGORITHM

UWB radars detect useful signals in the environment by transmitting pulse signals and receiving echo signals from the receiver. As shown in Figure 1, the radar typically does not sample the received echo signals during pulse transmission. Therefore, it is a "blind area" in the range of 0-R1 in Figure 1. In the detection range of R1-R2, sampling and storage are performed every Ts time as one frame of signal [36]. The data in the range of R1-R2 sampled by a pulse is called fast-time signal. When the UWB radar periodically sends multiple pulses, the dimension of the pulse number is called the slow-time signal. As shown in Figure 2, the radar echo signal is a three-dimensional data. The fast-time signal and the slow-time signal can be extracted from the data separately. When the transmitted pulse signal of the UWB radar

is reflected back by the human body, the radar echo signal is affected not only by the distance from the human body to the antenna, but also by the periodic motion of the chest caused by vital signs [37]. Due to the periodic motion of the lungs and heart, the chest cavity also periodically expands and contracts. Therefore, the radar echo signal carries the original distance information as well as vital sign information such as respiration and heartbeat [38]. The distance information of the radar transmission signal can be expressed as:

$$d(t) = d_0 + m_b sin(2\pi f_b t) + m_h sin(2\pi f_h t) \tag{1}$$

where m_b and m_h are the amplitudes of the respiration and heartbeat signals, f_b and f_h are the frequencies of the respiration and heartbeat signals. The radar echo signal can be expressed as:

$$r(t,\tau) = \sum_i A_i p(\tau - \tau_i) + Ap(\tau - \tau_d(t)) \tag{2}$$

$$\tau_d(t) = 2d(t)/c = \tau_0 + \tau_b sin(2\pi f_b t) + \tau_h sin(2\pi f_h t) \tag{3}$$

where $p(t)$ is the normalized pulse signal of the received signal. A and $\tau_d(t)$ are the amplitude and the phase delay of the multipath component reflected by humen body, A_i and τ_i are the amplitude and phase delay of the other multipath components reflected by the background. As can be seen from the formula (2), the multipath components reflected by the background are independent of slow-time t. These components correspond to the DC-component in slow-time. Therefore the background clutter contained in the echo signal can be removed by filtering.

$$x(t,\tau) = Ap(\tau - \tau_d(t)) + noise \tag{4}$$

where $x(t,\tau)$ is the filtered echo signal and *noise* is the residual error contained in the filtered echo signal. Due to the operation of removing error points in the algorithm steps, the residual error does not affect the algorithm judgment. Therefore, the small errors are ignored.

$$y(t,\tau) = x(t,\tau) - noise = Ap(\tau - \tau_d(t)) \tag{5}$$

According to the two-dimensional Fourier transform, the results are as follows:

$$\begin{aligned} Y(f,\nu) &= \int_{-\infty}^{\infty}\int_{-\infty}^{\infty} y(t,\tau)e^{-j2\pi ft}e^{-j2\pi\nu\tau}dtd\tau \\ &= \int_{-\infty}^{\infty}\int_{-\infty}^{\infty} Ap(\tau - \tau_d(t))e^{-j2\pi\nu\tau}e^{-j2\pi ft}dtd\tau \end{aligned} \tag{6}$$

According to the calculation rule of double integral, it can be seen that the simplification result is as follows:

$$Y(f,\nu) = AP(\nu)\int_{-\infty}^{\infty} e^{-j2\pi\nu\tau_d(t)}e^{-j2\pi ft}dt \tag{7}$$

where $P(\nu)$ is the Fourier transform of $p(\tau)$. To further simplify the formula, we can use the following Bessel function:

$$e^{-jzsin(2\pi f_0 t)} = \sum_{k=-\infty}^{\infty} J_k(z)e^{-j2\pi kf_0 t} \tag{8}$$

According to formula (3), (7) and (8), the final result of $Y(f,\nu)$ is as follows:

$$\begin{aligned} Y(f,\nu) = AP(\nu)e^{-j2\pi\nu\tau_0}\int_{-\infty}^{\infty}(\sum_{k=-\infty}^{\infty} J_k(\beta_b\nu)e^{-j2\pi kf_b t}) \\ \cdot(\sum_{k=-\infty}^{\infty} J_k(\beta_h\nu)e^{-j2\pi kf_h t})e^{-j2\pi ft}dt \end{aligned} \tag{9}$$

where $\beta_b = 2\pi m_b$ and $\beta_h = 2\pi m_h$. According to the Fourier transform formula and formula (9), $Y(f,\tau)$ is as follows:

$$\begin{aligned} Y(f,\tau) &= \int_{-\infty}^{\infty} Y(f,\nu)e^{j2\pi\nu\tau}d\nu \\ &= A\sum_{k=-\infty}^{\infty}\sum_{l=-\infty}^{\infty} G_{kl}(\tau)\delta(f - kf_b - lf_h) \end{aligned} \tag{10}$$

where the $G_{kl}(\tau)$ can be given as follws:

$$G_{kl}(\tau) = \int_{-\infty}^{\infty} P(\nu)J_k(\beta_b\nu)J_l(\beta_h\nu)e^{j2\pi\nu(\tau-\tau_0)}d\nu \tag{11}$$

The slow-time signal can represent the distance information. In the scene where the human body is detected the respiratory and heartbeat in a static state, the intensity of the human echo signal is the largest value, so when $\tau = \tau_0$, the $G_{kl}(\tau_0)$ is the maximum value. Therefore, $Y(f,\tau_0)$ can be expressed as follows [35]:

$$Y(f,\tau_0) = A\sum_{k=-\infty}^{\infty}\sum_{l=-\infty}^{\infty} C_{kl}\delta(f - kf_b - lf_h) \tag{12}$$

where C_{kl} is the maximum value of $G_{kl}(\tau)$ at $\tau = \tau_0$. Due to the characteristics of the pulse signal δ, it is clear that the frequency of the echo signal is: $f = kf_b + lf_h$. Therefore, the components of the echo signal contain the fundamental and harmonics of f_b,f_h and their intermodulation products. When $l = 0$, the echo frequency f only has the respiratory frequency, and the Kth harmonic of the respiratory signal is represented as $f_{b_k} = kf_b$. Similarly, when $k = 0$, the Lth harmonic of the heartbeat signal is expressed as $f_{h_l} = lf_h$. Since both k and l are integers, the Nth harmonic of the breath or heartbeat is N times the fundamental.

Since the amplitude of the harmonics is greatly attenuated from the second harmonic, more than three harmonics are masked by the environmental noise in the actual measurement results. In pursuit of higher algorithm accuracy and lower algorithm complexity, the HMLD algorithm only use the principle that the second harmonic is twice the fundamental wave to estimate the respiratory and heartbeat frequencies. The flow chart of the HMLD algorithm are shown in Figure 3. Firstly we use a band-pass filter(BPF) to intercept the frequency range of the fundamental signal. Since the fundamental component of the respiration and heartbeat is larger in the spectral range, we extract the peak frequency in the fundamental spectrum as the pending fundamental frequency. Similarly, we select the peak frequency of the second harmonic spectrum as the pending harmonic frequency. The pending fundamental frequency and pending harmonic

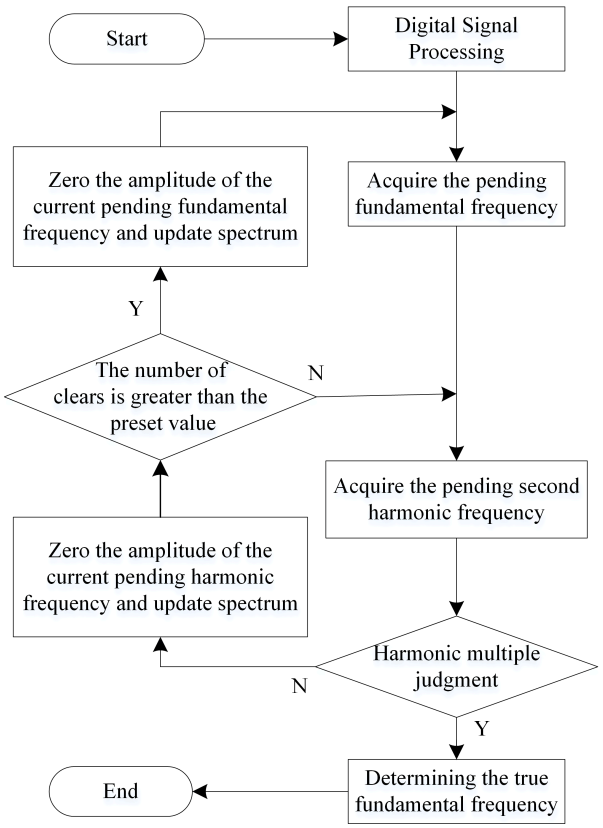

FIGURE 3. Harmonic multiple loop detection (HMLD) algorithm flow chart.

frequency are discriminated by using the principle of second harmonic multiple detection. Due to the influence of noise and intermodulation components, there may be a slight offset between the fundamental wave and the harmonic frequency. Therefore, we set an appropriate error to ensure the detection rate. If the result satisfies the principle of harmonic multiple detection, the pending fundamental frequency is the estimated frequency of the algorithm. Otherwise, the loop detection process is executed. The pending harmonic frequency are cleared and counted, and the corresponding frequency amplitudes in the spectrum are also cleared and updated. The HMLD algorithm looks for new pending harmonic components in the updated spectrum. The algorithm flow repeats the steps of getting the pending second harmonic. If the loop count value reaches the preset value, it is determined that the pending fundamental frequency is erroneous. Then the pending fundamental frequency is subjected to loop detection processing. The pending fundamental frequency and the spectrum are cleared and updated. The algorithm flow repeats the steps of getting pending fundamental frequency.

Since the HMLD algorithm reduces the detection processing of higher harmonic components, it has strong environmental robustness and low requirement of radar hardware. In addition, the HMLD algorithm does not need to set a threshold. It reduces the path unrecognizable and noise interference caused by the threshold setting and improves the detection accuracy. Due to fluctuations in the fundamental and harmonic frequencies, sometimes the true fundamental and second harmonic frequencies are not the maximum of the corresponding frequency bands. If only the harmonic multiple discrimination method is used, it may cause misjudgment. Therefore, we add loop detection processing based on the harmonic multiple discrimination to eliminate the erroneous pending fundamental and harmonic frequency to ensure the accuracy of the algorithm. In real-time detection, the HMLD algorithm simplifies discrimination principle and calculatio, which also reduces time of real-time detection.

TABLE 1. Biometric data of the subjects.

Subjects	Sex	Age	Weight	Height	Chest Circumference
S1	M	24	68Kg	181cm	94cm
S2	M	25	56Kg	165cm	90cm
S3	M	26	66.5Kg	173cm	95cm
S4	M	32	96Kg	183cm	102cm
S5	M	53	95Kg	175cm	101cm
S6	F	24	56Kg	172cm	80cm
S7	F	25	51Kg	160cm	87cm
S8	F	25	50Kg	160cm	86cm
S9	F	26	75Kg	168cm	96cm
S10	F	45	60Kg	163cm	89cm

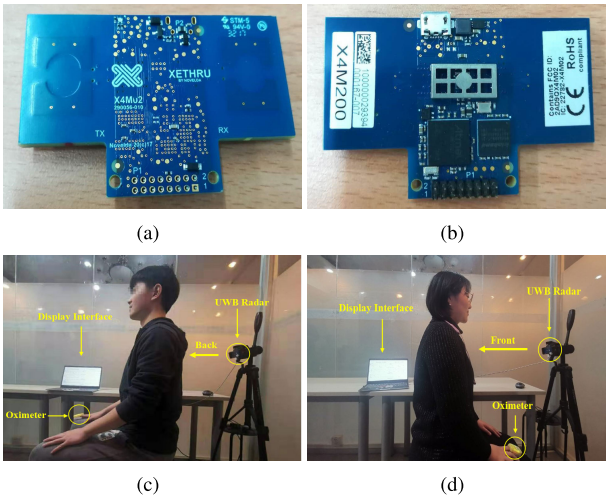

FIGURE 4. Non-contact vital sign detection experimental equipment and scenarios (a) Front side of UWB radar module (b) Back side of UWB radar module (c) Backward measurement scenario (d) Forward measurement scenario.

III. EXPERIMENTS AND METHODS

The measurements were conducted with 10 subjects which contains 5 males and 5 females respectively. The situation of all subjects is shown in TABLE 1. The subjects are in a sitting state to complete the vital signs detection from the front and back. Experimental equipment and test scenarios are shown in Figure 4. Subjects detected the real RR by chest wall cycle counting. And the real HR of subjects were detected by the pulse oximeter as shown in Figure 4. The radar transceiver is Novelda's radar sensor powered by the XeThru X4 system on chip [39]. The radar module with

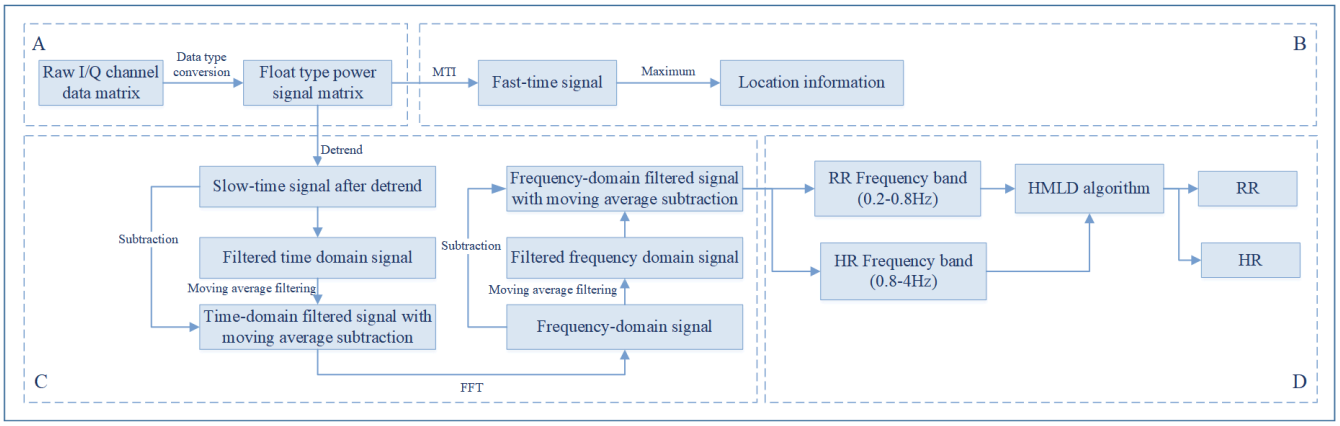

FIGURE 5. Flow chart of real-time vital sign detection system based on HMLD algorithm.

detection range up to 5 meters has a power consumption of less than 10mW and a bandwidth of a UWB frequency range. We can get 17 baseband frames per second from the radar module. After amplifying and downconverting the baseband signal, the orthogonal baseband components I(t) and Q(t) are analyzed to extract the desired vital sign signal [37], [39].

In the digital signal processing step, the I/Q channel signal is combined into the power signal [39]. The experiment selected two data blocks as a group, which have the same time length and time domain data overlapping 75% [30]. A detrend processing is performed on two data blocks to remove most of the interference of environmental clutter as shown in Figure 8. The two processed time domain data blocks are then subjected to fast Fourier transform to obtain two spectral data blocks. The two spectral data blocks are averaged to obtain more accurate approximate sampled data. In the actual measurement, the samples number of the fast Fourier transform is set to 1024. Due to the peak position error caused by spectral interference, an error of 0.05 is set in the discrimination of the harmonic multiple. During the measurement process, there may be an error in the extraction of harmonic components. Here we set the preset cycles number to 10 times.

The experimental content includes two parts: algorithm accuracy experiment and real-time detection experiment. The algorithm accuracy experiment used the data recording software provided by Novelda to record the sample data and perform offline digital signal processing on the sample. The length of the experimental sample is divided into 5 different intervals between 20-60 seconds. Each subject was tested on the front and back sides to obtain RR and HR samples for different time periods. The results and errors obtained by the sampled data through the HMLD algorithm are calculated to evaluate the accuracy of the algorithm. The error is calculated as follows [16]:

$$Error = \frac{1}{N}\sum \frac{|HR_{ref} - HR_{meas}|}{|HR_{ref}|} \times 100\% \qquad (13)$$

where HR_{ref} is the true value of the sample measured by pulse count, HR_{meas} is the estimated value of the sample, and N is the number of samples. Figure 5 shows the flow chart of the real-time detection experiment. The experimental steps are divided into four parts corresponding to ABCD of Figure 5. Part A converts the radar echo matrix into a decimal three-dimensional matrix as shown in Figure 2. And the matrix is decomposed into fast-time signals and slow-time signals by dimensions. The distance information of the subjects will be calculated from the fast-time signals in Part B. First we can use the moving target indicator (MTI) filter to remove background clutter from the original three-dimensional signal [40], [41]. Then we get the subject's location information by extracting the peak value. Part C is the real-time filtering process. The two filtered slow-time data blocks that overlap by 75% are selected for averaging processing to form the average data block. The average data block is filtered by the time domain subtraction processing of moving average filtering. The filtered signal is subjected to Fast Fourier transform and then filtered by the frequency domain subtraction processing of moving average filtering. The respiratory band and the heartbeat band are respectively input into the HMLD algorithm in part D. Therefore, we can obtain the real-time RR,HR and location information of subjects through the real-time vital sign detection system.

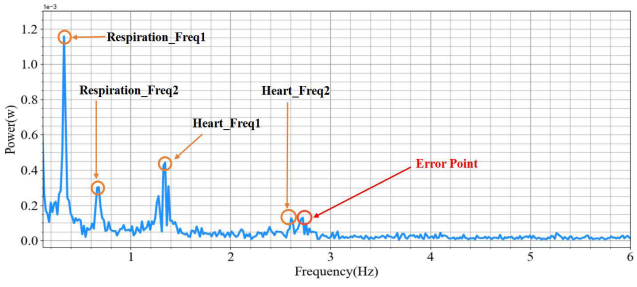

FIGURE 6. Spectrum of adjacent data blocks with a duration of 60s.

IV. RESULTS

A. ALGORITHM ACCURACY EXPERIMENT

Figure 6 shows the average spectrogram for a duration of 60s. The four orange circles represent the pending fundamental

TABLE 2. Comparison of the Noncontact HR measurements with different detection systems and algorithms.

Papers	Published Year	Radar	Algorithm	Vital Signs	Direction	RR Error (%)	HR Error (%)
[3]	2019	UWB	An Improved Convolutional Sparse Coding Algorithm	HR	Front	NA	1.9-6.6
[23]	2018	UWB	Variational mode decomposition (VMD)	RR/HR	Front	<5	<13
[30]	2018	UWB, Body-coupled antennas	Power spectral density(PSD)	RR/HR	Back	NA	1.82-5.21
			Spectrum-averaged harmonic path algorithm(SHAPA)			NA	2.22-6.62
			State space method(SSM)			NA	3.36-7.13
[27]	2017	UWB	Find the highest frequency of FFT spectrogram	RR/HR	Front	<10	<5
[35]	2016	UWB	MTI filter and finding the highest frequency of the spectrogram	RR/HR	Front	<5	NA
This paper		UWB	Harmonic multiple loop detection algorithm(HMLD)	RR/HR	Front	<5.28	<5.83
					Back	<5.44	<5.45

and second harmonic components of the respiration and heartbeat. The red circle is the error point rejected by the loop mechanism. In Figure 6, we can observe that the pending fundamental and second harmonic components of respiration is 0.332 Hz and 0.68Hz.The multiple error value is calculated by the harmonic multiple judgment standard and is 0.048, which is within the error range of 0.05. The real RR is 0.34Hz, so the test error of RR is 1.176%. The pending heartbeat fundamental frequency of the 0.8-2 Hz band is 1.345 Hz. The first peak of the 2-4 Hz band is 2.761 Hz. The multiple error calculated from the pending fundamental frequency is 0.0527. The error range is not satisfied, so the error point is removed by the loop mechanism. The second peak is 2.702, and the multiple error of 0.008 satisfies the error range, so the heartbeat frequency estimated by the algorithm is 1.345. Compared with the real respiratory rate of 1.35, the test error of HR is 0.37%.

FIGURE 7. The average errors for different time periods. The figure above is for women, and the figure below is for men. Blue and orange represent forward and backward RR errors, and gray and golden yellow represent forward and backward measured HR errors.

Among 1000 groups of data in the algorithm accuracy experiment, 99.6% of the data were effectively estimated by HMLD algorithm. It can be seen that the characteristics of extracting only second harmonics and fundamentals and removing threshold setting improve the effective estimation rate of HMLD algorithm. Figure 7 shows the average errors of the HMLD algorithm for male and female in different time periods of 20-60s. As can be seen from Figure 7, both men and women can effectively detect RR and HR through the HMLD algorithm. TABLE 2 shows a error comparison of the proposed method with several other typical non-contact vital sign measurement approaches based on UWB radar. As can be seen from the data in the TABLE 2, the RR errors of most algorithms are below 10% and the HR errors of most algorithms are in the range of 1.82%-13%. The RR and HR average errors of the HMLD algorithm are 4.95% and 5.06%. Therefore, TABLE 2 proves that the proposed method achieves a convincing performance among these papers. The above results show that the HMLD algorithm can correct the error that the path is unrecognizable caused by the weak radar echo signal, and improve the accuracy of the algorithm detection and the estimation of heartbeat frequency in the actual measurement environment.

B. REAL-TIME DETECTION EXPERIMENT

In the real-time vital sign detection experiment, we calculated the distance information and vital sign information of the subject by the HMLD algorithm. Figure 8 shows the original radar echo image and the image processed by MTI filter in 1 second. It can be seen from Figure 8 that the MTI filter removes most of the environmental noise and makes the effective signal clearer. We can calculate that the subject is at a distance of 0.64m from the radar by obtaining the average peak of multiple sets of data. Figure 9 shows the display interface for real-time vital sign detection. The interface displays the distance information, the 32-second respiratory time domain signal, the 50-second real-time RR and the 50-second real-time HR. Subjects can observe real-time changes in their location and vital sign information from real-time systems. Therefore, it is shown that the HMLD algorithm can accurately estimate the frequency of vital signs and display the current frequency and historical data in real time. The loop processing in the HMLD algorithm can

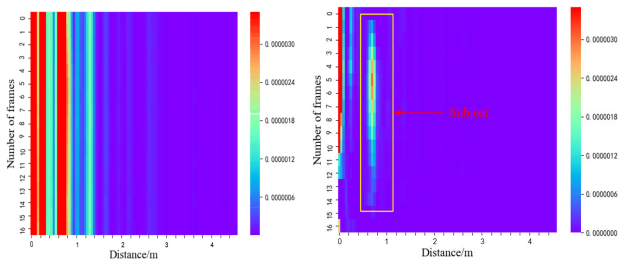

FIGURE 8. Comparison of radar echo images within one second before and after MTI processing. The left image is the original echo image, and the right image is the image processed by MTI.

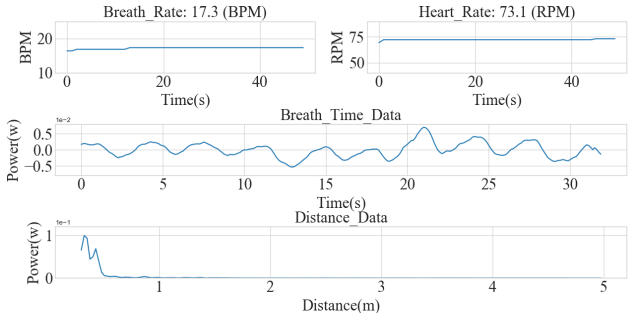

FIGURE 9. Real-time non-contact vital sign detection display interface with distance information, respiratory time domain waveform, and rate of respiration and heartbeat.

remove the invalid spectrum information in time, and return information to remind the subject adjusting the detection angle and distance. In addition, due to the low complexity of the HMLD algorithm, the detection processing time is also shortened. The experimental data proves that the HMLD algorithm has the advantages of high detection rate and high precision and can also achieve accurate real-time vital sign detection.

V. CONCLUSION

In this paper, a new low-complexity algorithm, HMLD, is proposed to detect the rate of respiration and heartbeat utilizing IR-UWB radar. The algorithm is elaborated and demonstrated through algorithm accuracy experiments and real-time detection experiments. The results prove that the algorithm can realize real-time non-contact vital sign detection while ensuring high accuracy and high detection. Because the proposed algorithm only needs to detect the fundamental and second harmonic components of the vital sign signal to obtain the rate of respiration and heartbeat, the effective estimation rate is 99.6%. In the algorithm accuracy experiment, the RR and HR average errors of the proposed algorithm are 4.95% and 5.06% respectively. In the real-time detection experiment, the rate of respiration and heartbeat, the change curve of real-time detection and the location information are recorded on the display interface, which also proves that the proposed algorithm is effective in real-time detection of HR, RR and distance information.The real-time system based on the HMLD algorithm realizes non-contact vital sign detection while protecting the privacy of the subjects, which solves the problem of inconvenient vital sign detection of special patients.

REFERENCES

[1] H. Hong, L. Zhang, H. Zhao, H. Chu, C. Gu, M. Brown, X. Zhu, and C. Li, "Microwave sensing and sleep: Noncontact sleep-monitoring technology with microwave biomedical radar," *IEEE Microw. Mag.*, vol. 20, no. 8, pp. 18–29, Aug. 2019.

[2] V. L. Petrovic, M. M. Jankovic, A. V. Lupsic, V. R. Mihajlovic, and J. S. Popovic-Bozovic, "High-accuracy real-time monitoring of heart rate variability using 24 GHz continuous-wave Doppler radar," *IEEE Access*, vol. 7, pp. 74721–74733, 2019.

[3] P. Wang, F. Qi, M. Liu, F. Liang, H. Xue, Y. Zhang, H. Lv, and J. Wang, "Noncontact heart rate measurement based on an improved convolutional sparse coding method using IR-UWB radar," *IEEE Access*, vol. 7, pp. 158492–158502, 2019.

[4] C. Li, Z. Peng, T.-Y. Huang, T. Fan, F.-K. Wang, T.-S. Horng, J.-M. Munoz-Ferreras, R. Gomez-Garcia, L. Ran, and J. Lin, "A review on recent progress of portable short-range noncontact microwave radar systems," *IEEE Trans. Microw. Theory Techn.*, vol. 65, no. 5, pp. 1692–1706, May 2017.

[5] L. Rose and S. P. Clarke, "Vital signs," *Amer. J. Nursin*, vol. 110, no. 5, p. 11, 2010.

[6] S. Wu, T. Sakamoto, K. Oishi, T. Sato, K. Inoue, T. Fukuda, K. Mizutani, and H. Sakai, "Person-specific heart rate estimation with ultra-wideband radar using convolutional neural networks," *IEEE Access*, vol. 7, pp. 168484–168494, 2019.

[7] E. M. Staderini, "UWB radars in medicine," *IEEE Aerosp. Electron. Syst. Mag.*, vol. 17, no. 1, pp. 13–18, Jan. 2002.

[8] H. Ghanadian, M. Ghodratigohar, and H. Al Osman, "A machine learning method to improve non-contact heart rate monitoring using an RGB camera," *IEEE Access*, vol. 6, pp. 57085–57094, 2018.

[9] W. Wang, A. C. Den Brinker, and G. De Haan, "Single-element remote-PPG," *IEEE Trans. Biomed. Eng.*, vol. 66, no. 7, pp. 2032–2043, Jul. 2019.

[10] G. Bai, J. Huang, and H. Liu, "Real-time robust noncontact heart rate monitoring with a camera," *IEEE Access*, vol. 6, pp. 33682–33691, 2018.

[11] S. Sanyal and K. K. Nundy, "Algorithms for monitoring heart rate and respiratory rate from the video of a user's face," *IEEE J. Transl. Eng. Health Med.*, vol. 6, 2018, Art. no. 2700111.

[12] J. C. Cobos Torres and M. Abderrahim, "Measuring heart and breath rates by image photoplethysmography using wavelets technique," *IEEE Latin Amer. Trans.*, vol. 15, no. 10, pp. 1864–1868, Oct. 2017.

[13] W. Karlen, A. Garde, D. Myers, C. Scheffer, J. M. Ansermino, and G. A. Dumont, "Estimation of respiratory rate from photoplethysmographic imaging videos compared to pulse oximetry," *IEEE J. Biomed. Health Informat.*, vol. 19, no. 4, pp. 1331–1338, Jul. 2015.

[14] H.-Y. Wu, M. Rubinstein, E. Shih, J. Guttag, F. Durand, and W. Freeman, "Eulerian video magnification for revealing subtle changes in the world," *ACM Trans. Graph.*, vol. 31, no. 4, pp. 1–8, Jul. 2012.

[15] L. Ren, L. Kong, F. Foroughian, H. Wang, P. Theilmann, and A. E. Fathy, "Comparison study of noncontact vital signs detection using a Doppler stepped-frequency continuous-wave radar and camera-based imaging photoplethysmography," *IEEE Trans. Microw. Theory Techn.*, vol. 65, no. 9, pp. 3519–3529, Sep. 2017.

[16] M. Li and J. Lin, "Wavelet-Transform-Based Data-Length-Variation technique for fast heart rate detection using 5.8-GHz CW Doppler radar," *IEEE Trans. Microw. Theory Techn.*, vol. 66, no. 1, pp. 568–576, Jan. 2018.

[17] J. Tu and J. Lin, "Fast acquisition of heart rate in noncontact vital sign radar measurement using Time-Window-Variation technique," *IEEE Trans. Instrum. Meas.*, vol. 65, no. 1, pp. 112–122, Jan. 2016.

[18] L. Ren, H. Wang, K. Naishadham, Q. Liu, and A. E. Fathy, "Non-invasive detection of cardiac and respiratory rates from stepped frequency continuous wave radar measurements using the state space method," in *IEEE MTT-S Int. Microw. Symp. Dig.*, May 2015, pp. 1–4.

[19] M. Mercuri, Y.-H. Liu, I. Lorato, T. Torfs, F. Wieringa, A. Bourdoux, and C. Van Hoof, "A direct phase-tracking Doppler radar using wavelet independent component analysis for non-contact respiratory and heart rate monitoring," *IEEE Trans. Biomed. Circuits Syst.*, vol. 12, no. 3, pp. 632–643, Jun. 2018.

[20] A. D. Droitcour, "Non-contact measurement of heart and respiration rates with a single-chip microwave Doppler radar," Ph.D. dissertation, Dept. Elect. Eng., Stanford Univ., Stanford, CA, USA, 2006.

[21] C. Li, J. Ling, J. Li, and J. Lin, "Accurate Doppler radar noncontact vital sign detection using the RELAX algorithm," *IEEE Trans. Instrum. Meas.*, vol. 59, no. 3, pp. 687–695, Mar. 2010.

[22] Z. Zhang, Y. Li, K. Mouthaan, and Y. Lian, "A miniature mode reconfigurable inductorless IR-UWB transmitter–receiver for wireless short-range communication and vital-sign sensing," *IEEE J. Emerg. Sel. Topic Circuits Syst.*, vol. 8, no. 2, pp. 294–305, Jun. 2018.

[23] Z. Duan and J. Liang, "Non-contact detection of vital signs using a UWB radar sensor," *IEEE Access*, vol. 7, pp. 36888–36895, 2019.

[24] P. Withington, H. Fluhler, and S. Nag, "Enhancing homeland security with advanced UWB sensors," *IEEE Microw. Mag.*, vol. 4, no. 3, pp. 51–58, Sep. 2003.

[25] K.-K. Shyu, L.-J. Chiu, P.-L. Lee, T.-H. Tung, and S.-H. Yang, "Detection of breathing and heart rates in UWB radar sensor data using FVPIEF-based two-layer EEMD," *IEEE Sensors J.*, vol. 19, no. 2, pp. 774–784, Jan. 2019.

[26] P. Bernardi, R. Cicchetti, S. Pisa, E. Pittella, E. Piuzzi, and O. Testa, "Design, realization, and test of a UWB radar sensor for breath activity monitoring," *IEEE Sensors J.*, vol. 14, no. 2, pp. 584–596, Feb. 2014.

[27] R. El-Bardan, D. Malaviya, and A. Di Rienzo, "On the estimation of respiration and heart rates via an IR-UWB radar: An algorithmic perspective," in *Proc. IEEE Int. Conf. Microw., Antennas, Commun. Electron. Syst. (COMCAS)*, Nov. 2017, pp. 1–5.

[28] D. T. Wisland, K. Granhaug, J. R. Pleym, N. Andersen, S. Stoa, and H. A. Hjortland, "Remote monitoring of vital signs using a CMOS UWB radar transceiver," in *Proc. 14th IEEE Int. New Circuits Syst. Conf. (NEWCAS)*, Jun. 2016, pp. 1–4.

[29] V. Nguyen, A. Q. Javaid, and M. A. Weitnauer, "Harmonic path (HAPA) algorithm for non-contact vital signs monitoring with IR-UWB radar," in *Proc. IEEE Biomed. Circuits Syst. Conf. (BioCAS)*, Oct. 2013, pp. 146–149.

[30] V. Nguyen, A. Q. Javaid, and M. A. Weitnauer, "Spectrum-averaged harmonic path (SHAPA) algorithm for non-contact vital sign monitoring with ultra-wideband (UWB) radar," in *Proc. 36th Annu. Int. Conf. IEEE Eng. Med. Biol. Soc.*, Aug. 2014, pp. 2241–2244.

[31] E. Schires, P. Georgiou, and T. S. Lande, "Vital sign monitoring through the back using an UWB impulse radar with body coupled antennas," *IEEE Trans. Biomed. Circuits Syst.*, vol. 12, no. 2, pp. 292–302, Apr. 2018.

[32] T. Sakamoto, M. Muragaki, K. Tamura, S. Okumura, T. Sato, K. Mizutani, K. Inoue, T. Fukuda, and H. Sakai, "Measurement of instantaneous heart rate using radar echoes from the human head," *Electron. Lett.*, vol. 54, no. 14, pp. 864–866, Jul. 2018.

[33] Y. Xu, S. Dai, S. Wu, J. Chen, and G. Fang, "Vital sign detection method based on multiple higher order cumulant for ultrawideband radar," *IEEE Trans. Geosci. Remote Sens.*, vol. 50, no. 4, pp. 1254–1265, Apr. 2012.

[34] L. Ren, Y. S. Koo, H. Wang, Y. Wang, Q. Liu, and A. E. Fathy, "Noncontact multiple heartbeats detection and subject localization using UWB impulse Doppler radar," *IEEE Microw. Wireless Compon. Lett.*, vol. 25, no. 10, pp. 690–692, Oct. 2015.

[35] L. Ren, H. Wang, K. Naishadham, O. Kilic, and A. E. Fathy, "Phase-based methods for heart rate detection using UWB impulse Doppler radar," *IEEE Trans. Microw. Theory Techn.*, vol. 64, no. 10, pp. 3319–3331, Oct. 2016.

[36] Y.-H. Liu, S. Sheelavant, M. Mercuri, P. Mateman, and M. Babaie, "An ultralow power burst-chirp UWB radar transceiver for indoor vital signs and occupancy sensing in 40-nm CMOS," *IEEE Solid-State Circuits Lett.*, vol. 2, no. 11, pp. 256–259, Nov. 2019.

[37] L. Ren and A. E. Fathy, "Noncontact heartbeat detection using UWB impulse Doppler radar," in *Proc. USNC-URSI Radio Sci. Meeting (Joint with AP-S Symp.)*, Jul. 2015, pp. 1–3.

[38] A. Lazaro, D. Girbau, and R. Villarino, "ANALYSIS OF VITAL SIGNS MONITORING USING AN IR-UWB RADAR," *Prog. Electromagn. Res.*, vol. 100, pp. 265–284, 2010.

[39] *x4m200 Datasheet*. Accessed: Oct. 18, 2018. [Online]. Available: https://www.xethru.com/x4m200-respiration-sensor.html/

[40] S. Kim and K.-K. Lee, "Low-complexity joint Extrapolation-MUSIC-Based 2-D parameter estimator for vital FMCW radar," *IEEE Sensors J.*, vol. 19, no. 6, pp. 2205–2216, Mar. 2019.

[41] A. Lazaro, D. Girbau, R. Villarino, and A. Ramos, "Vital signs monitoring using impulse based UWB signal," in *Proc. 41st Eur. Microw. Conf.*, Oct. 2011, pp. 135–138.

YI ZHANG received the B.Eng. degree in communication engineering from Zhengzhou University, Zhengzhou, China, in 2017. She is currently pursuing the master's degree in electronic and communication engineering with the Beijing University of Posts and Telecommunications, Beijing, China. Her current research interest includes radar signal processing.

XIUPING LI (Senior Member, IEEE) received the B.S. degree from Shandong University, in 1996, and the Ph.D. degree from the Beijing Institute of Technology, in 2001.

From 2001 to 2003, she joined the Positioning and Wireless Technology Center, Nanyang Technological University, Singapore, where she was a Research Fellow and involved in the research and development of RFID systems. In 2003, she was a Research Professor with Yonsei University, Seoul, South Korea. Since 2004, she has been an Associate Professor with the Beijing University of Posts and Telecommunications, Beijing, China, and promoted to Professor, in 2009. She is currently the Vice Dean of the School of Electronic Engineering, Beijing University of Posts and Telecommunications. She is the author of four books and over 100 journal articles and conference papers. She holds more than 20 PRC patents. Her current research interests include millimeter-wave antennas, terahertz (THz) antennas, RFID systems, and MMIC systems.

RUI QI received the B.Eng. degree in electronic and information engineering from Yangtze University, Jingzhou, China, in 2018. He is currently pursuing the master's degree in electronic and communication engineering with the Beijing University of Posts and Telecommunications, Beijing, China.

ZIHANG QI (Student Member, IEEE) received the B.E. degree in electronic and information engineering from China Three Gorges University, Yichang, China, in 2013, and the Ph.D. degree in electronic science and technology from the Beijing University of Posts and Telecommunications, Beijing, China, in 2019. He is currently a Postdoctoral Fellow with the Beijing University of Posts and Telecommunications. His current research interests include OAM antennas, millimeter-wave/terahertz (THz) antennas, and microwave filters. He was a recipient of the 2018 National Scholarship of China for Doctoral Students.

HUA ZHU (Member, IEEE) received the M.S. degree from the Guilin University of Electronic Technology, Guilin, China, in 2010, and the Ph.D. degree from the Beijing University of Posts and Telecommunications, Beijing, China, in 2015. She is currently a Lecturer with the Beijing University of Posts and Telecommunications. Her research interests include UHF RFID beam scanning antenna array design in complex environment and millimeter-wave/terahertz antenna design.